Front. Phys., 2014, 9(6): 774–779
DOI 10.1007/s11467-013-0353-5

RESEARCH ARTICLE

Electronic transport through tetrahedron-structured DNA-like system

Wei Zhu, Ai-Min Guo†, Qing-Feng Sun

Institute of Physics, Chinese Academy of Sciences, Beijing 100190, China

E-mail: †aimin.guo218@gmail.com

Received March 1, 2013; accepted May 25, 2013

We theoretically investigate the electronic transport properties of a multi-terminal tetrahedron-structured DNA under a uniform magnetic field. Based on a tight-binding model, the current and nonlocal resistance are calculated under different situations by employing the Landauer–Büttiker formula. Our results indicate that the current displays a clear sign of interference in the presence of the magnetic field and can be mainly divided into three patterns, as demonstrated by the Fourier transformation. Furthermore, the tetrahedron-structured DNA can be used as a molecular switch. The underlying physical mechanisms are analyzed for the various phenomena observed in this three-dimensional DNA interferometer.

Keywords tetrahedron structure, interference, AB effect

PACS numbers 87.14.gk, 85.65.+h, 87.15.Pc, 72.80.-r

1 Introduction

The charge transport properties of the DNA molecules have attracted extensive attention during the last years. Since Eley and Spivey first suggested that the DNA may conduct charge carriers [1], it has been expected to be a fascinating material in the research field of nanoelectronics. The DNA has great self-assembly property which allows us to make various three-dimensional (3D) structures and can be synthesized in any specific sequence. These important features have spurred many experiments to study the electronic transport properties of the DNA. However, the experimental results are quite different that the DNA could be insulator [2–5], semiconductor [6–9], conductor [10–13], or even induced superconductor [14]. These controversial results can be traced back to the intrinsic and extrinsic experimental complications, including the DNA samples, humidity, counterions, and the coupling between the DNA and the electrode [15]. Recently, it has been reported that perfectly packed double-stranded DNA (dsDNA) monolayer can transport electrons over 34 nm efficiently [16]. Furthermore, the dsDNA can be also used as a spin filter with high spin polarization at room temperature [17–19]. And the spin filtration efficiency could be controlled by varying the DNA length, the sequence, and the gate voltage [20, 21]. This property indicates that the dsDNA is an excellent candidate for spintronics.

Nevertheless, there is a major problem about the dsDNA monolayer, that is the crowding effect. Since the dsDNA cannot stay upright on the electrode, there will be phase segregation, interstrand entanglement, end-to-end collision and some of the dsDNA will bend toward the electrode [22–24]. Such a drawback will affect the charge transport efficiency and prevent us from investigating the electronic properties of the dsDNA precisely. A 3D DNA, namely the tetrahedron-structured DNA, has been designed to avoid this drawback of the dsDNA [25, 26]. Because of its robust structure, the monolayer of the tetrahedron-structured DNA can not only hold back the crowding effect, but also transport electrons with high efficiency [24]. Besides, for its fabulous properties, the tetrahedron-structured DNA possesses a promising future to be used in various areas: (i) It can be an important platform for biosensing [27]. The tetrahedron-structured probe has better sensitivity than single-stranded DNA (ssDNA), and the sensitivity can be improved as much as 250-fold. It also has excellent selectivity of single-base mismatch for the target DNA. In contrast to the ssDNA probe, the tetrahedron-structured DNA probe can be widely used in biological

fluids such as serum owing to its protein-prevent property [27]. Based on these great properties, quite a lot of work has been down to use this kind of probe in different areas [28, 29]. (ii) Moreover, very recently, Walsh *et al.* reported that the hollow structure of the tetrahedron-structured DNA could make it a great nanoscale material for delivering and controlling cargoes (e.g., medicine) within the cells in biology [30]. The experiment showed that the uptake of the tetrahedron-structured DNAs into the cells could happen without help from other materials and they could stay intact in the cells for at least 48 hours [30]. And further experiment showed that the tetrahedron-structured DNAs which were appended with un-methylated cytosine-phosphate-guanine motifs could induce the secretion of cytokines when they were in the cells [31]. Though with these advantages, the tetrahedron-structured DNA can be synthesised quickly and reliably with high yield. However, to our knowledge, no theoretical work has been done about the tetrahedron-structured DNA.

In this paper, we explore the electronic transport properties of the tetrahedron-structured DNA in the presence of a uniform magnetic field by combining the Landauer–Büttiker formula and nonequilibrium Green function method. The current and nonlocal resistance are studied. The current shows clear sign of interference and has classic Aharonov–Bohm period. Besides, other properties of the current are also described and can be proved, for which the tetrahedron-structured DNA can be used as molecular switch, 3D interferometer, etc.

The rest of the paper is organized as follows: In Section 2, we present the theoretical model with parameters determined by the first-principles calculations. In Section 3, the current and nonlocal resistance are studied under different conditions. Finally, we give our conclusion about the results in Section 4.

2 Model

In our model, six same ssDNAs with no helix make up of the tetrahedron. And the whole tetrahedron-structured DNA only consists of one kind of nucleobase with a uniform magnetic field perpendicular to the bottom surface (see Fig. 1). The Hamiltonian can be written as

$$\mathcal{H}=\sum_{j=1}^{6}\left(\sum_{i=1}^{N}\varepsilon_{ji}a_{ji}^{\dagger}a_{ji}+\sum_{i=1}^{N-1}t_{ji}\mathrm{e}^{\mathrm{i}\Phi_{i,i+1}}a_{ji}^{\dagger}a_{ji+1}+\mathrm{H.c.}\right) \tag{1}$$

where $a_{ji}^{\dagger}$ and a_{ji} are, respectively, the creation and annihilation operators at site i of the jth ssDNA, ε_{ji} is the on-site energy and t_{ji} is the hopping integral. The perpendicular magnetic field brings a phase $\Phi_{i,i+1}$ to the hopping element between two neighboring sites, and its expression is $\Phi_{i,i+1}=\int_{i}^{i+1}\boldsymbol{A}\cdot\mathrm{d}\boldsymbol{l}/\Phi_0$ with $\Phi_0=h/e$. Each vertex of the tetrahedron-structured DNA is contacted by a normal metal electrode. The current in the pth lead can be calculated from the Landauer–Büttiker formula [32]: $I_p=(2e^2/h)\sum_m T_{pm}(V_m-V_p)$ and V_p is the voltage in the pth lead. Through nonequilibrium Green function we can express the transmission coefficient as $T_{pm}=\mathrm{Tr}[\Gamma_p\boldsymbol{G}^r\Gamma_m\boldsymbol{G}^a]$ with the Green functions $\boldsymbol{G}^r=[\boldsymbol{G}^a]^{\dagger}=[E\boldsymbol{I}-\boldsymbol{H}-\sum_p\Sigma_p^r]^{-1}$ and the linewidth functions $\Gamma_p=\mathrm{i}[\Sigma_p^r-\Sigma_p^a]$. Here E is the Fermi energy, $\boldsymbol{I}$ is an identity matrix and Σ_p^r (Σ_p^a) is the retarded (advanced) self-energy which describes the coupling to the pth lead. By taking the wide bandwidth approximation [33, 34], the retarded and advanced self-energies are as follows: $\Sigma_p^r=[\Sigma_p^a]^{\dagger}=-\mathrm{i}\Gamma_p/2$. In this model we set $\varepsilon_{ji}=0$ and $t_{ji}=0.1$, which are determined by first-principles calculations [35–37]. Also we fix $\Gamma_p=0.1$.

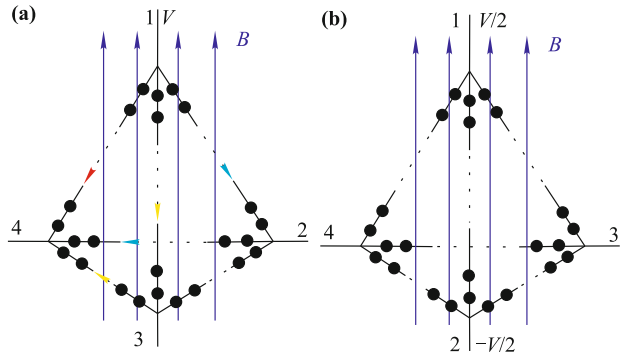

Fig. 1 Schematic views of the tetrahedron-structured DNA with different boundary conditions. The full circles represent the nucleobases. A uniform magnetic field is applied to be perpendicular to the bottom surface and each vertex of the tetrahedron-structured DNA is connected to a lead. **(a)** A voltage V is applied in the first lead and the voltages are 0 in the other three leads. **(b)** Two voltages $V/2$ and $-V/2$ are applied in the first and second leads, respectively, and the currents are 0 in the other two leads.

Two conditions are concerned for this model: (i) A voltage V is applied in the first lead and the voltages in the bottom three leads are 0 [see Fig. 1(a)]. Due to the symmetry of the structure, the currents in the bottom three leads are all the same. (ii) A bias V is applied between the first and second leads, which leads a current flowing from the first lead through the tetrahedron-structured DNA to the second lead. The third and fourth leads are set as the voltage probe with currents being zero. In fact, these two different situations will show identical quantum interference properties. Therefore, we will only give the flux-dependent current for situation (i), which is more closer to the experiment [27].

3 Results and discussion

Let us first investigate the condition (i). Figure 2 plots current versus the Fermi energy E for two different lengths. One notes the energy spectrum consists of peaks which are almost of the same height. More peaks appear [see Fig. 2(b)] by lengthening the ssDNA and the number of the peaks is nearly proportional to the length. This is because more energy states emerge as the ssDNA becomes longer.

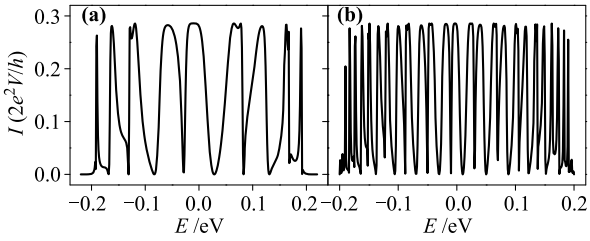

Fig. 2 Energy-dependent current in one of the bottom leads for **(a)** $n = 10$ and **(b)** $n = 30$ by fixing $\Phi = 0.25\Phi_0$. Here, n is the number of nucleobases in a ssDNA of the tetrahedron and Φ represents the magnetic flux through one side triangle of the tetrahedron.

We then focus on the electronic transport properties of the tetrahedron-structured DNA under a perpendicular magnetic field. Figure 3 shows current vs. magnetic flux for several values of Fermi energy with different lengths. One notes that the current oscillates with the magnetic flux in different patterns. It is a clear sign of interference for the different electron paths in the system due to the influence of the magnetic flux. However, the current curves are quite dissimilar for different lengths and energy values, they do share some characteristics according to the high symmetry of this structure. For instance, the most obvious feature is that the current has a period of Φ_0, it can be expressed as $I(\Phi) = I(\Phi + \Phi_0)$ as illustrated in the figure. This is classic AB period, and for which we can just investigate the current curves in a period of Φ_0. Furthermore, for a certain length with different Fermi energy, three patterns are distinguishable of the current curves: (1) the current oscillates once in a period; (2) the current oscillates twice in a period; (3) peaks appear in a period. And curves for other energy values can be included into these three patterns as well. Besides, to further explore the underlying meaning of these three patterns, Fourier transformation is introduced below. Apart from this, the flux-dependent current also possesses other properties which may not seem quite obvious. First $I(\Phi) = I(-\Phi)$, which reveals the current will not be affected by reversing the magnetic field. Second $I(\Phi) = I(k\Phi_0 - \Phi)$ with k the integer, this formula can be seen as the extended version of the first one. By fixing $k = 0$, the first formula can be easily derived. Moreover, the second feature shows the curve is centred at $\Phi = k\Phi_0/2$ as illustrated in the figure. All the properties mentioned above can be demonstrated analytically. In addition, another major property of the tetrahedron-structured DNA arouses our attention. For a given length, the current changes sharply with the flux under a specific Fermi energy (see Fig. 3). That means a small alteration in the magnetic flux will lead to a sudden jump in the current from zero to a finite value or the reverse. Accordingly, the tetrahedron-structured DNA is a promising material for molecular switch. In our model, the current is formed by electrons hopping between neighboring nucleobases. So when the number of nucleobases along each edge of the tetrahedron is changed, the resonant energies will be shifted and the current at a fixed Fermi energy should be dissimilar. Thus for different lengths, the switchable current appears under different Fermi energies. Moreover, other kinds of molecular switch can be achieved by fixing the magnetic flux while changing the Fermi energy or length.

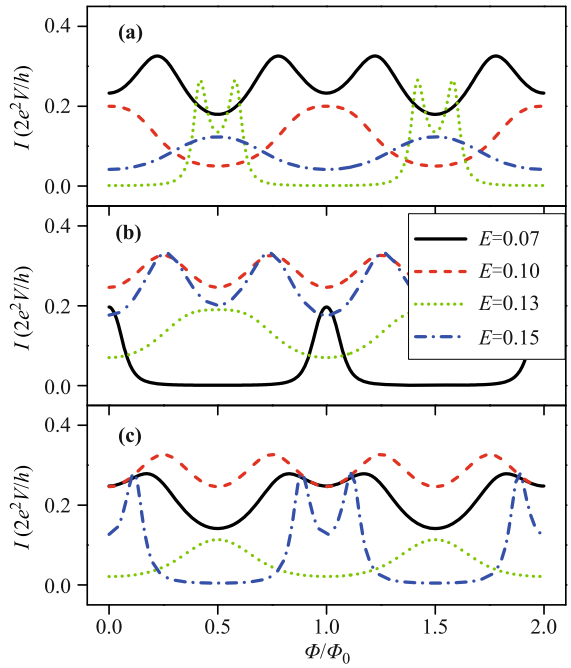

Fig. 3 Flux-dependent current for **(a)** $n = 10$, **(b)** $n = 30$, and **(c)** $n = 60$ with several values of Fermi energy E.

In order to investigate the implied meaning of the three patterns of the flux-dependent current curves, Fourier transformation is introduced to do the spectrum analyse. The transform expression is as follows:

$$A_M = \left| \int_0^{\Phi_0} I(\Phi) \mathrm{e}^{-\mathrm{i}M\Phi} \mathrm{d}\Phi \right| \tag{2}$$

Here A_M represents amplitude, M is integer which means harmonic frequency. We focus on the tetrahedron-structured DNA with $n = 30$ [see Fig. 3(b)], for three different Fermi energy values which correspond to the three patterns of the current curves we give the results of the Fourier transformation (see Fig. 4). One clearly notices three distinct different situations: (i) the amplitude of the first harmonic wave is much larger than the others, indicating one oscillation in a period Φ_0; (ii) the amplitude of the second harmonic wave is much larger than the others, which leads to two oscillation in a period; (iii) the amplitude of the first several harmonic waves are all quite large and close, then peaks appear due to the addition of these waves. Besides, the results of Fourier transformation for the current curves with $n = 10$ and $n = 60$ can be included into the three situations as well. Apart from the apparent differences, one can notice that the amplitudes of the first and second harmonic waves are always quite large in all three situations. This phenomenon can be explained as follows. In Fig. 1(a), the shortest and most possible three electron paths from the first lead to the fourth are labeled by the arrows with different colours. If just considering these three paths, the transmission coefficient can be written as $T_{41} = |t_1 + t_1 t_2 e^{i\Phi} + t_1 t_2 e^{-i\Phi}|^2$ with t_1 and t_2 being the transmission amplitudes from the terminal 1 to other terminal and between two terminals of the bottom surface, respectively. This transmission coefficient T_{41} is the main part of the real transmission coefficient. By expanding the expression of T_{41}, one can clearly see it is made up of the first and second harmonic waves. Since the current is proportional to the transmission coefficient, we can have above conclusion. However, due to the reflection in the leads, more electron paths appear and the interference becomes very complicated which leads to the appearance of high frequency harmonic waves.

At last we consider the boundary condition (ii) and study the nonlocal resistance R, where $R = (V_4 - V_3)/(I_2 - I_1)$. Now two different voltages $V/2$ and $-V/2$ are applied in the first and second leads with the magnetic field still the same as before [see Fig. 1(b)]. The boundary condition is that the currents in the third and fourth leads are 0. Fig. 5 shows the nonlocal resistance versus the magnetic flux for three different lengths. Here we have $R(\Phi) = R(\Phi + \Phi_0)$, the period still keeps the same which is determined by AB effect [see Fig. 5]. The resistance curves all have four oscillations in a period, irrespective of the lengths. In addition, the curves for $n = 30$ and $n = 60$ are quite the same as illustrated in the figure. We compare the two curves and find they are almost superpose, which indicates somehow at first the resistance changes with the length but it becomes saturate as the length gets longer. Furthermore, for some special points on the curves the resistance can be 0, this is because the voltage between the two leads is 0 on these occasions.

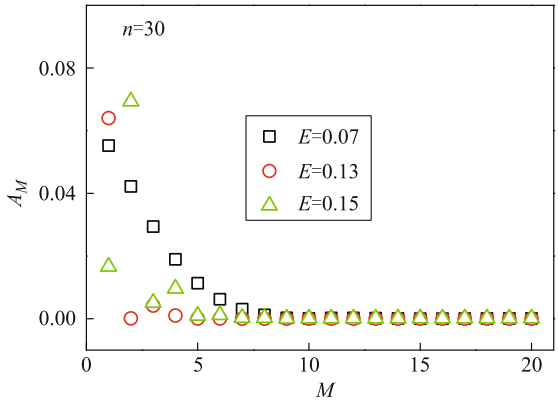

Fig. 4 Fourier transformation of the currents in Fig. 3(b). Here M is integer which means the harmonic frequency and A_M represents the amplitude.

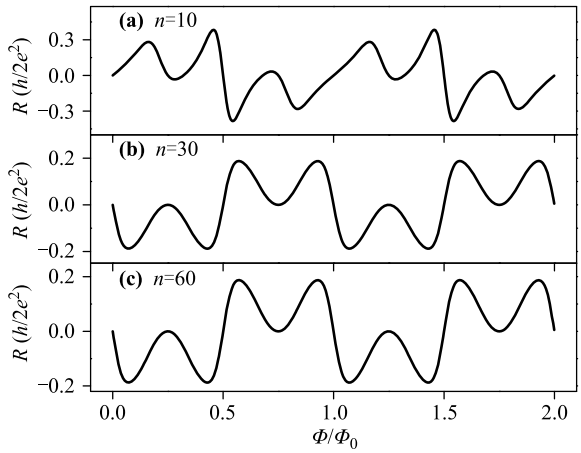

Fig. 5 Flux-dependent nonlocal resistance of the tetrahedron-structured DNA with different DNA length n. The nonlocal resistance can be expressed as $R = (V_4 - V_3)/(I_2 - I_1)$.

4 Conclusion

In summary, we investigate the electronic transport properties of the tetrahedron-structured DNA under the influence of a magnetic field. Due to the AB effect and the high symmetry of the structure, the magnetic flux-dependent current shows some special properties. One special property of this DNA structure makes it a perfect material for molecular switch. We also give the magnetic flux-dependent nonlocal resistance under another situation and give a basic description.

Acknowledgements This work was financially supported by NBRP of China (2012CB921303 and 2009CB929100) and NSF-

China under Grants Nos. 11074174 and 11274364.

References

1. D. D. Eley and D. I. Spivey, Semiconductivity of organic substances. Part 9. Nucleic acid in the dry state, *Trans. Faraday Soc.*, 1962, 58: 411
2. E. Braun, Y. Eichen, U. Sivan, and G. Ben-Yoseph, DNA-templated assembly and electrode attachment of a conducting silver wire, *Nature*, 1998, 391(6669): 775
3. P. J. de Pablo, F. Moreno-Herrero, J. Colchero, J. Gómez Herrero, P. Herrero, A. M. Baró, P. Ordejón, J. M. Soler, and E. Artacho, Absence of dc-conductivity in lambda-DNA, *Phys. Rev. Lett.*, 2000, 85(23): 4992
4. A. J. Storm, J. van Noort, S. de Vries, and C. Dekker, Insulating behavior for DNA molecules between nanoelectrodes at the 100 nm length scale, *Appl. Phys. Lett.*, 2001, 79(23): 3881
5. Y. Zhang, R. H. Austin, J. Kraeft, E. C. Cox, and N. P. Ong, Insulating behavior of lambda-DNA on the micron scale, *Phys. Rev. Lett.*, 2002, 89(19): 198102
6. H. Cohen, C. Nogues, R. Naaman, and D. Porath, Direct measurement of electrical transport through single DNA molecules of complex sequence, *Proc. Natl. Acad. Sci. USA*, 2005, 102(33): 11589
7. M. S. Xu, R. G. Endres, S. Tsukamoto, M. Kitamura, S. Ishida, and Y. Arakawa, Conformation and local environment dependent conductance of DNA molecules, *Small*, 2005, 1(12): 1168
8. E. Shapir, H. Cohen, A. Calzolari, C. Cavazzoni, D. A. Ryndyk, G. Cuniberti, A. Kotlyar, R. Di Felice, and D. Porath, Electronic structure of single DNA molecules resolved by transverse scanning tunnelling spectroscopy, *Nat. Mater.*, 2008, 7(1): 68
9. S. Roy, H. Vedala, A. D. Roy, D. H. Kim, M. Doud, K. Mathee, H. K. Shin, N. Shimamoto, V. Prasad, and W. Choi, Direct electrical measurements on single-molecule genomic DNA using single-walled carbon nanotubes, *Nano Lett.*, 2008, 8(1): 26
10. H. W. Fink and C. Schönenberger, Electrical conduction through DNA molecules, *Nature*, 1999, 398(6726): 407
11. P. Tran, B. Alavi, and G. Gruner, Charge transport along the lambda-DNA double helix, *Phys. Rev. Lett.*, 2000, 85(7): 1564
12. L. Cai, H. Tabata, and T. Kawai, Probing electrical properties of oriented DNA by conducting atomic force microscopy, *Nanotechnology*, 2001, 12(3): 211
13. B. Xu, P. Zhang, X. Li, and N. Tao, Direct conductance measurement of single DNA molecules in aqueous solution, *Nano Lett.*, 2004, 4(6): 1105
14. A. Y. Kasumov, M. Kociak, S. Guéron, B. Reulet, V. T. Volkov, D. V. Klinov, and H. Bouchiat, Proximity-induced superconductivity in DNA, *Science*, 2001, 291(5502): 280
15. R. G. Endres, D. L. Cox, and R. R. P. Singh, Colloquium: The quest for high-conductance DNA, *Rev. Mod. Phys.*, 2004, 76(1): 195
16. J. D. Slinker, N. B. Muren, S. E. Renfrew, and J. K. Barton, DNA charge transport over 34 nm, *Nat. Chem.*, 2011, 3(3): 228
17. B. Göhler, V. Hamelbeck, T. Z. Markus, M. Kettner, G. F. Hanne, Z. Vager, R. Naaman, and H. Zacharias, Spin selectivity in electron transmission through self-assembled monolayers of double-stranded DNA, *Science*, 2011, 331(6019): 894
18. Z. Xie, T. Z. Markus, S. R. Cohen, Z. Vager, R. Gutierrez, and R. Naaman, Spin specific electron conduction through DNA oligomers, *Nano Lett.*, 2011, 11(11): 4652
19. A. M. Guo and Q. F. Sun, Spin-selective transport of electrons in DNA double helix, *Phys. Rev. Lett.*, 2012, 108(21): 218102
20. A. M. Guo and Q. F. Sun, Sequence-dependent spin-selective tunneling along double-stranded DNA, *Phys. Rev. B*, 2012, 86(11): 115441
21. A. M. Guo and Q. F. Sun, Enhanced spin-polarized transport through DNA double helix by gate voltage, *Phys. Rev. B*, 2012, 86(3): 035424
22. K. J. Cash, F. Ricci, and K. W. Plaxco, An electrochemical sensor for the detection of protein-small molecule interactions directly in serum and other complex matrices, *J. Am. Chem. Soc.*, 2009, 131(20): 6955
23. A. A. Gorodetsky and J. K. Barton, Electrochemistry using self-assembled DNA monolayers on highly oriented pyrolytic graphite, *Langmuir*, 2006, 22(18): 7917
24. N. Lu, H. Pei, Z. L. Ge, C. R. Simmons, H. Yan, and C. H. Fan, Charge transport within a three-dimensional DNA nanostructure framework, *J. Am. Chem. Soc.*, 2012, 134(32): 13148
25. R. P. Goodman, R. M. Berry, and A. J. Turberfield, The single-step synthesis of a DNA tetrahedron, *Chem. Commun.*, 2004, (12): 1372
26. R. P. Goodman, I. A. T. Schaap, C. F. Tardin, C. M. Erben, Rapid chiral assembly of rigid DNA building blocks for molecular nanofabrication, *Science*, 2005, 310(5754): 1661
27. H. Pei, N. Lu, Y. Wen, S. Song, Y. Liu, H. Yan, and C. H. Fan, A DNA nanostructure-based biomolecular probe carrier platform for electrochemical biosensing, *Adv. Mater.*, 2010, 22(42): 4754
28. H. Pei, Y. Wan, J. Li, H. Y. Hu, Y. Su, Q. Huang, and C. H. Fan, Regenerable electrochemical immunological sensing at DNA nanostructure-decorated gold surfaces, *Chem. Commun.*, 2011, 47(22): 6254
29. Y. L. Wen, H. Pei, Y. Wan, Y. Su, Q. Huang, S. P. Song, and C. H. Fan, DNA nanostructure-decorated surfaces for enhanced aptamer-target binding and electrochemical cocaine sensors, *Anal. Chem.*, 2011, 83(19): 7418

30. A. S. Walsh, H. Yin, C. M. Erben, M. J. Wood, and A. J. Turberfield, DNA cage delivery to mammalian cells, *ACS Nano*, 2011, 5(7): 5427

31. J. Li, H. Pei, B. Zhu, L. Liang, M. Wei, Y. He, N. Chen, D. Li, Q. Huang, and C. H. Fan, Self-assembled multivalent DNA nanostructures for noninvasive intracellular delivery of immunostimulatory CpG oligonucleotides, *ACS Nano*, 2011, 5(11): 8783

32. S. Datta, Electronic transport in Mesoscopic Systems, Cambridge: Cambridge University Press, 1995

33. Q. F. Sun, J. Wang, and T. H. Lin, Photon sidebands of the ground state and the excited state of a quantum dot: A nonequilibrium Green-function approach, *Phys. Rev. B*, 1998, 58(19): 13007

34. Q. F. Sun and X. C. Xie, Bias-controllable intrinsic spin polarization in a quantum dot: Proposed scheme based on spin-orbit interaction, *Phys. Rev. B*, 2006, 73(23): 235301

35. H. Zhang, X. Q. Li, P. Han, X. Y. Yu, and Y. Yan, A partially incoherent rate theory of long-range charge transfer in deoxyribose nucleic acid, *J. Chem. Phys.*, 2002, 117(9): 4578

36. K. Senthilkumar, F. C. Grozema, C. F. Guerra, F. M. Bickelhaupt, F. D. Lewis, Y. A. Berlin, M. A. Ratner, and L. D. A. Siebbeles, Absolute rates of hole transfer in DNA, *J. Am. Chem. Soc.*, 2005, 127(42): 14894

37. L. G. D. Hawke, G. Kalosakas, and C. Simserides, Electronic parameters for charge transfer along DNA, *Eur. Phys. J. E*, 2010, 32(3): 291